Characterization of Mechanical Properties of a Synthetic Modeling Clay Used as a Substitute for Natural Soils

Hyunjin Lee,[1] Nitish Ponkshe,[2] James P. Hambleton, Ph.D., M.ASCE,[3] and James D. Van de Ven, Ph.D.[4]

[1]Department of Civil and Environmental Engineering, Northwestern University, Room A236, 2145 Sheridan Road, Evanston, IL 60208; E-mail: hyunjinlee2021@northwestern.edu
[2]Department of Mechanical Engineering, University of Minnesota, 111 Church Street SE, Minneapolis, MN 55455; E-mail: ponks001@umn.edu
[3]Department of Civil and Environmental Engineering, Room A236, 2145 Sheridan Road, Northwestern University, Evanston, IL 60208; E-mail: jphambleton@northwestern.edu
[4]Department of Mechanical Engineering, University of Minnesota, 111 Church Street SE, Minneapolis, MN 55455; E-mail: vandeven@umn.edu

ABSTRACT

This paper discusses the use of Crayola modeling clay as a substitute for natural soil. This product is relatively inexpensive, non-drying, reusable, pliable, and commercially available. The unconfined compression test was performed to determine mechanical properties. Additionally, inverse analysis was implemented to characterize the elastoplastic response. The model used in the inverse analysis considers finite deformation plasticity. The stress-strain relationship was obtained by defining a local dissipation function and using the principle of maximum dissipation. The formulation is based on hyperelasticity and expressed in terms of Kirchhoff stress, logarithmic strain, and the multiplicative decomposition of deformation gradient to overcome the limitations of the theory based on infinitesimal deformation. The hardening behavior is prescribed based on Ludwik's equation. Inverse analysis is performed using a genetic algorithm to minimize the difference between the experimental data and predicted results for the unconfined compression tests.

INTRODUCTION

The negative implications of time, cost, sample preparation difficulty, and moisture fluctuation are major barriers in the use of natural soil samples for physical modeling, both in conventional laboratories and centrifuge testing facilities. In order to overcome these disadvantages, there is increasing demand for artificial clay that is cost effective and allows for repeatable experiments with easily controlled moisture content. As an alternative to natural soils, a variety of materials have been used to create artificial soil samples. For imitating natural soil, POM

(polyoxymethylene) beads, glass beads of various sizes, and sawdust, which combine to form aggregates having the size of natural soil aggregates, have been used in soil penetration for nature-inspired robotics (Tonazzini et al. 2012; A. Sadeghi et al. 2013, 2014; Del Dottore et al. 2016; Mishra et al. 2018). Additionally, transparent synthetic soil consisting of silica gel and amorphous silica was made by Iskander et al. (1994) to visualize deformation inside a soil body during laboratory tests.

This work aims to characterize the mechanical properties of Crayola modeling clay as an artificial soil using an unconfined compression test. In particular, this paper presents a methodology for the characterization of mechanical properties via inverse analysis. Sample preparation and the experimental results obtained through unconfined compression testing are first described. Next, a framework based on finite elastoplasticity combined with Ludwik's strain-hardening model is introduced to describe the plastic behavior of the modeling clay. Subsequently, an inverse procedure using a genetic algorithm to match the experimental measurement is presented. Finally, estimated material parameters from inverse analysis are presented and evaluated using a finite element model.

MATERIAL AND EXPERIMENTS

Crayola modeling clay is selected as an alternative to natural soil due to its malleability and non-drying attributes. A 453 g box of commercially available Crayola modeling clay is composed of four cuboidal clay slabs of different colors. To obtain a homogeneous sample, 14 boxes are mixed thoroughly by hand. This mixture is placed in a cylindrical mold with an inner diameter of 197 mm, and then it is compressed with a platen such that the modeling clay conforms to the geometry of the mold. The final cylindrical sample has a height of 125 mm and a diameter of 197 mm.

To examine the basic mechanical behavior of the modeling clay, an unconfined compression test (UCT) was performed according to D211/D2166M ASTM under three different loading rates: 1.42, 10, and 100 mm/min. Two specimens were prepared in the form of a right circular cylinder of diameter 34.8 mm and 71.1 mm in height for each loading rate condition. The experimental setup is shown in Figure 1(a). The response of force-displacement is given in Figure 1(b), which shows the response is rate-dependent. Noticeably, a transition to plastic behavior is observable after approximately 5 mm of displacement.

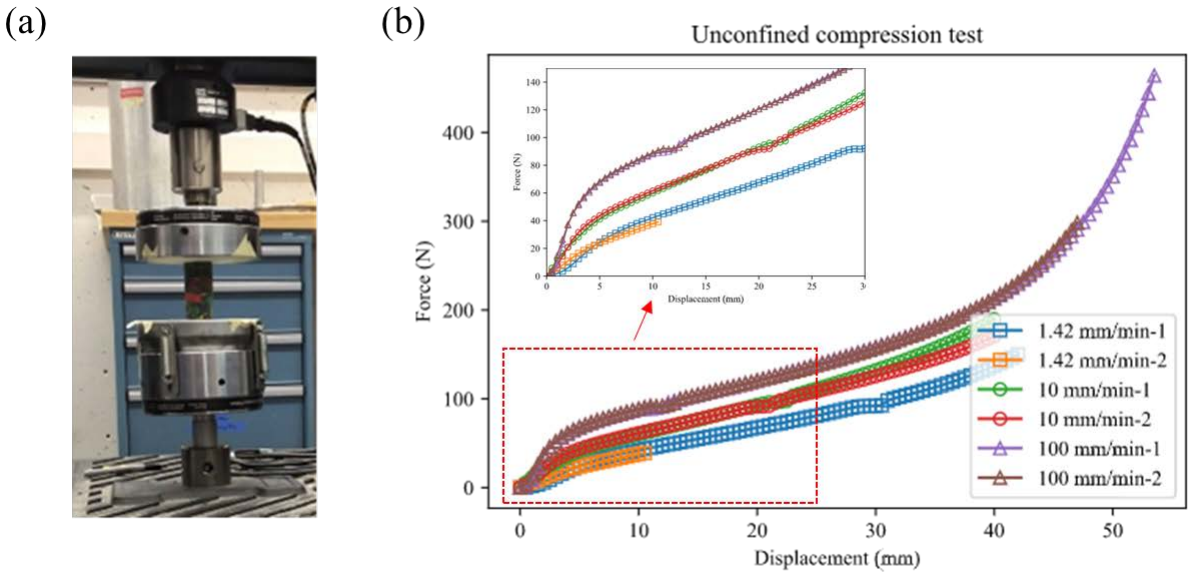

Figure 1. (a) Unconfined compression test setup. (b) Force-displacement response of UCT under 1.42, 10 and 100 mm/min loading rates.

FINITE ELASTOPLASTICITY

Among the various methods for resolving many difficulties associated with finite deformation, Simo (1992, 1993) proposed the framework of finite plasticity, which preserves the classical return-mapping algorithm of infinitesimal theory. This method is adopted to describe the finite elastoplastic behavior of the modeling clay, and the formulations are summarized in this section.

Multiplicative decomposition. The multiplicative decomposition theory is used to overcome the assumption of the infinitesimal theory, which uses an additive decomposition of the strain and strain rate. This theory assumes that there exists an intermediate configuration so that the deformation gradient $\mathbf{F}(\mathbf{X})$ can be decomposed into elastic and plastic deformation gradients as follows:

$$\mathbf{F}(\mathbf{X}) = \mathbf{F}^{\mathrm{e}}(\mathbf{X})\mathbf{F}^{\mathrm{p}}(\mathbf{X}) \tag{1}$$

where $\mathbf{F}^{\mathrm{p}}(\mathbf{X})$ is an internal variable related to the amount of plastic flow and $\mathbf{F}^{\mathrm{e}-1}(\mathbf{X})$ defines the local, stress-free, unloaded process.

Stress measure and elastic domain. For finite deformation, plasticity models are typically formulated in the current configuration. To describe the evolution of stress and that of deformation of multiplicative plasticity, the elastic domain can be defined in the Kirchhoff stress space by

$$E = \{(\boldsymbol{\tau}, \mathbf{q}) | \, f(\boldsymbol{\tau}, \mathbf{q}) \leq 0\} \tag{2}$$

$$\boldsymbol{\tau} = J\boldsymbol{\sigma} \tag{3}$$

where $\boldsymbol{\tau}$ is the Kirchhoff stress tensor and differs from the Cauchy stress tensor $\boldsymbol{\sigma}$ by a factor of $J = \det(\mathbf{F})$. The yield function f restricts to isotropy and is expressed in terms of $\boldsymbol{\tau}$ and $\mathbf{q}$, the latter being a vector of stress-like plastic variables.

Dissipation inequality and constitutive equations. The free energy represents stored energy by elastic deformation and is independent of the orientation. Thus, it can be written in terms of the right or left Cauchy-Green deformation tensor, such as the strain energy density. Since the deformation in elastoplasticity is composed of elastic and plastic parts, the free energy function can be defined as

$$\psi = \psi(\mathbf{b}^{\mathrm{e}}, \boldsymbol{\xi}) \tag{4}$$

$$\mathbf{q} = -\frac{\partial \psi}{\partial \boldsymbol{\xi}} \tag{5}$$

where $\mathbf{b^e} \equiv \mathbf{F^e F^{e^T}}$ is the elastic left Cauchy-Green deformation tensor and $\boldsymbol{\xi}$ is the vector of strain-like plastic variables conjugate to $\mathbf{q}$**.** Local dissipation function D is a nonnegative function and is expressed as the difference between the stress power and the rate of change in free energy as follows:

$$D \equiv \boldsymbol{\tau} : \mathbf{d} - \frac{d}{dt}\psi(\mathbf{b}^{\mathrm{e}}, \boldsymbol{\xi}) \geq 0 \tag{6}$$

where $\mathbf{d} = \mathrm{sym}(\mathbf{L})$ is the rate of deformation and $\mathbf{L} = \dot{\mathbf{F}}\mathbf{F^{-1}}$ is the velocity gradient. The constitutive relation can be obtained by expanding a local dissipation function via the chain rule with a time derivative of the elastic left Cauchy-Green deformation tensor:

$$\dot{\mathbf{b}}^{\mathrm{e}} = \mathbf{L}\mathbf{b}^{\mathrm{e}} + \mathbf{b}^{\mathrm{e}}\mathbf{L}^{\mathrm{T}} + \mathrm{L_v}(\mathbf{b}^{\mathrm{e}}) \tag{7}$$

$$D = \left(\boldsymbol{\tau} - 2\frac{d\psi}{d\mathbf{b}^{e}}\mathbf{b^e}\right) : \mathbf{d} + \left(2\frac{d\psi}{d\mathbf{b}^{e}}\mathbf{b^e}\right) : \left[-\frac{1}{2}\,\mathrm{L_v}(\mathbf{b}^{\mathrm{e}})\mathbf{b}^{e^{-1}}\right] + \mathbf{q} \cdot \dot{\boldsymbol{\xi}} \geq 0 \tag{8}$$

where $\mathrm{L_v}(\mathbf{b}^{\mathrm{e}})$ is referred to as the Lie derivative of $\mathbf{b}^{\mathrm{e}}$. Since the inequality equation holds for all admissible stress and plastic variables, the following constitutive relation and reduced dissipation inequality can be obtained for arbitrary $\mathbf{d}$:

$$\boldsymbol{\tau} = 2\frac{d\psi}{d\mathbf{b}^{e}}\mathbf{b}^{\mathbf{e}} \tag{9}$$

$$D = \boldsymbol{\tau}\colon\left[-\frac{1}{2}\,\mathrm{L_v}(\mathbf{b}^{\mathrm{e}})\mathbf{b}^{e^{-1}}\right] + \mathbf{q}\cdot\dot{\boldsymbol{\xi}} \geq 0 \tag{10}$$

This is equivalent to saying that for all possible state variables within the elastic domain, the following inequality holds for arbitrary $\boldsymbol{\tau}^{*}$ and $\mathbf{q}^{*}$:

$$D = (\boldsymbol{\tau} - \boldsymbol{\tau}^{*})\colon\left[-\frac{1}{2}\,\mathrm{L_v}(\mathbf{b}^{\mathrm{e}})\mathbf{b}^{e-1}\right] + (\mathbf{q} - \mathbf{q}^{*})\cdot\dot{\boldsymbol{\xi}} \geq 0 \tag{11}$$

Evolution equations. The evolution equations can be expressed based on the normality to the yield surface with a plastic consistency parameter γ:

$$-\frac{1}{2}\,\mathrm{L_v}\mathbf{b}^{e} = \gamma\frac{\partial f(\boldsymbol{\tau},\mathbf{q})}{\partial\boldsymbol{\tau}}\mathbf{b}^{\mathbf{e}} \tag{12}$$

$$\dot{\boldsymbol{\xi}} = \gamma\frac{\partial f(\boldsymbol{\tau},\mathbf{q})}{\partial\mathbf{q}} \tag{13}$$

$$\gamma \geq 0, \qquad f(\boldsymbol{\tau},\mathbf{q}) \leq 0, \qquad \gamma f(\boldsymbol{\tau},\mathbf{q}) = 0 \tag{14}$$

The last equation is the same as the Kuhn-Tucker condition of classical elastoplasticity. Then the rate form of $\mathbf{b}^{\mathrm{e}}$ can be rewritten by substituting Eq. (12) into Eq. (7) as follows:

$$\dot{\mathbf{b}}^{\mathrm{e}} = [\mathbf{L}\mathbf{b}^{\mathrm{e}} + \mathbf{b}^{\mathrm{e}}\mathbf{L}^{\mathrm{T}}] - 2\gamma\frac{\partial f(\boldsymbol{\tau},\mathbf{q})}{\partial\boldsymbol{\tau}}\mathbf{b}^{\mathbf{e}} \tag{15}$$

The trial elastic left Cauchy-Green deformation tensor can be written by introducing the relative deformation gradient denoted by $\mathbf{f}$:

$$\mathbf{b}^{\mathrm{e,tr}} = \mathbf{f}\mathbf{b}^{\mathrm{e}}\mathbf{f}^{\mathrm{T}} \tag{16}$$

$$\mathbf{f} = \mathbf{F}(\mathbf{F}^{\mathrm{tr}})^{-\mathbf{1}} \tag{17}$$

The rate form of elastoplastic evolution needs to be integrated to calculate plastic variables using the trial state. By integrating the differential equation, the following return-mapping algorithm can be obtained:

$$\mathbf{b}^{\mathrm{e}} = \mathbf{b}^{\mathrm{e,tr}} \exp\left[-2\Delta\gamma \frac{\partial f(\boldsymbol{\tau}, \mathbf{q})}{\partial \boldsymbol{\tau}} \mathbf{b}^{\mathbf{e}}\right] \tag{18}$$

$$\boldsymbol{\xi} = \boldsymbol{\xi}^{tr} + \Delta\gamma \frac{\partial f(\boldsymbol{\tau}, \mathbf{q})}{\partial \mathbf{q}} \tag{19}$$

$$\Delta\gamma \geq 0, \qquad f(\boldsymbol{\tau}, \mathbf{q}) \leq 0, \qquad \Delta\gamma f(\boldsymbol{\tau}, \mathbf{q}) = 0 \tag{20}$$

Exponential return-mapping algorithms. For isotropic materials, the principal directions of $\boldsymbol{\tau}$ and $\mathbf{b}^{\mathrm{e}}$ coincide based on the isotropic assumption, and they can be reconstructed via spectral decomposition:

$$\mathbf{b}^{\mathrm{e}} = \sum_{i=1}^{3} \lambda_i^2 \boldsymbol{n}^i \otimes \boldsymbol{n}^i \tag{21}$$

$$\boldsymbol{\tau} = \sum_{i=1}^{3} \tau_i^p \boldsymbol{n}^i \otimes \boldsymbol{n}^i \tag{22}$$

where λ_i is the principal stretch, τ^p is the principal Kirchhoff stresses, and $\boldsymbol{n}^i$ is the spatial eigenvector. Additionally, we assume that the hardening behavior is uncoupled from the elastic deformation so that the free energy consists of the elastic stored energy through the so-called Henky model, which is formulated in terms of principal elastic strain:

$$\psi = \frac{1}{2}\lambda[e_1 + e_2 + e_3]^2 + \mu[e_1^2 + e_2^2 + e_3^2] + H(\boldsymbol{\xi}) \tag{23}$$

where $H(\boldsymbol{\xi})$ denotes energy from isotropic hardening law (the specific form of which is described in the next section) and λ and μ are Lame's constants. Since the equation of $\mathbf{b}^{\mathrm{e}}$ is not straightforward to implement, Simo proposed taking logarithms to simplify the expressions. With this, the exponential term will be converted into an additional form, and the strain $\mathbf{b}^{\mathrm{e}}$ will be the logarithmic strain e with the following relation:

$$e_i = \log(\lambda_i) \tag{24}$$

Using the above free energy and Simo's idea, the constitutive relation then becomes a linear relation between the principal Kirchhoff stresses and the principal logarithmic strain:

$$\boldsymbol{\tau}^{\mathrm{p}} = \frac{\partial \psi}{\partial \mathbf{e}} = \mathbf{c}^{\mathrm{e}}\mathbf{e} \tag{25}$$

where $\mathbf{c}^{\mathrm{e}} = \left(\lambda + \frac{2}{3}\mu\right)\mathbf{1} \otimes \mathbf{1} + 2\mu\mathbf{1}_{\mathrm{dev}}$ is the elastic constitutive tensor for an isotropic material. The following return-mapping algorithm can be obtained, which is identical to the classical return-mapping of the infinitesimal theory:

$$\boldsymbol{\tau}^{\mathrm{p,tr}} = \mathbf{c}^{\mathrm{e}}\mathbf{e}^{\mathbf{tr}} \tag{26}$$

$$\boldsymbol{\tau}^{\mathrm{p}} = \boldsymbol{\tau}^{\mathrm{p,tr}} - \Delta\gamma \boldsymbol{c}^{e} \frac{\partial f(\boldsymbol{\tau}^{\mathrm{p}}, \mathbf{q})}{\partial \boldsymbol{\tau}^{\mathrm{p}}} \tag{27}$$

$$\boldsymbol{\xi} = \boldsymbol{\xi}^{\boldsymbol{tr}} + \Delta\gamma \frac{\partial f(\boldsymbol{\tau}^{\mathrm{p}}, \mathbf{q})}{\partial \mathbf{q}} \tag{28}$$

$$\Delta\gamma \geq 0, \qquad f(\boldsymbol{\tau}, \mathbf{q}) \leq 0, \qquad \Delta\gamma f(\boldsymbol{\tau}, \mathbf{q}) = 0 \tag{29}$$

Hardening model. The stress-strain behavior of the synthetic modeling clay is adjusted to Ludwik's equation with the von Mises yield criterion. It is suitable to model the strain-hardening behavior observed in many paste-like materials. It can be written in the following form:

$$\sigma_y = \sigma_{y0} + K\left(\varepsilon_{eq}^{p}\right)^{n} \tag{30}$$

In this equation, K and n respectively represent the strain hardening modulus and the strain hardening exponent of the material. Variables σ_{y0} and ε_{eq}^{p} are the initial yield stress and the equivalent plastic strain in terms of true stress and true strain, respectively.

INVERSE ANALYSIS FOR CHARACTERIZATION

This study aims to characterize the mechanical properties of the modeling clay from the unconfined compression test under different loading rates. To determine the unknown material parameters of the proposed constitutive model, inverse analysis was implemented using a genetic algorithm (GA). In this study, force and displacement are important indicators to represent the mechanical behavior. Therefore, the error function should represent these two important indicators by taking the following expression:

$$Error(x) = \frac{1}{N}\sum_{i=1}^{N}\sqrt{\left(u_{exp}^{i} - u_{predict}^{i}\right)^{2}} \tag{31}$$

where u_{exp}^{i} and $u_{predict}^{i}$ are respectively the experimental and the predicted force values (the latter obtained using the trial parameter set) and N is the number of measured experimental values.

After defining the error function, the inverse analysis can be considered as the minimization of the error function. Given the fact that the error function becomes increasingly complex and non-differentiable in the multi-dimensional parameter space, it is difficult to determine whether the solution is the global minimum using gradient-based optimization techniques. Therefore, a genetic algorithm, which is a stochastic optimization technique conceived by simulating natural evolution, is adopted as an optimization method. Six operators of GA, consisting of population, evaluation fitness, selection, crossover, inversion, and mutation, proceed repeatedly until the optimal solution satisfies the convergence criterion.

To calculate the predicted value, the stress-strain behavior is computed based on the above finite elastoplasticity model at material level. Then, the force-displacement curve is determined based on the current configuration of the specimen's geometry as follows: (1) the displacement is converted into the velocity gradient as an input, and (2) the force is calculated at the current configuration as an output. The three material parameters of Ludwik's equation, as well as Young's modulus and Poisson's ratio, are determined as a result of the optimization.

RESULTS

Table 1 presents a summary of the estimated parameters determined through optimization. Poisson's ratio, the strain hardening modulus, and the strain hardening exponent are consistent over the different loading rates. However, the values of Young's modulus and the initial yield stress vary with different loading rates.

Figure 2 shows the comparison between the experimental data and the predicted force-displacement curve using the estimated parameters obtained from calculations at the material level. It can be observed that the estimated parameters with a proposed constitutive model give a good agreement. Additionally, unconfined compression tests are simulated using axisymmetric elements via ABAQUS to evaluate the estimated parameters for the full boundary-value problem. The proposed hardening law is implemented using a user-material subroutine (UMAT) available in ABAQUS. All finite element simulations are ended at 25 mm displacement due to convergence issues. A good correlation is achieved with a relatively small error over the three curves for each loading rate.

Table 1. Summary of estimated parameters.

Loading rates	Young's Modulus (kPa)	Poisson's ratio	Initial yield stress, $\boldsymbol{\sigma_{y0}}$ (kPa)	K (kPa)	n
1.42 mm/min	342 ± 39	0.38 ± 0.05	17 ± 7	46.5 ± 3	0.303 ± 0.001
10 mm/min	567 ± 45	0.31 ± 0.01	37 ± 2.9	49.4 ± 0.5	0.349 ± 0.049
100 mm/min	1219 ± 41	0.30 ± 0.01	50 ± 0.5	50.1 ± 0.2	0.300 ± 0.001

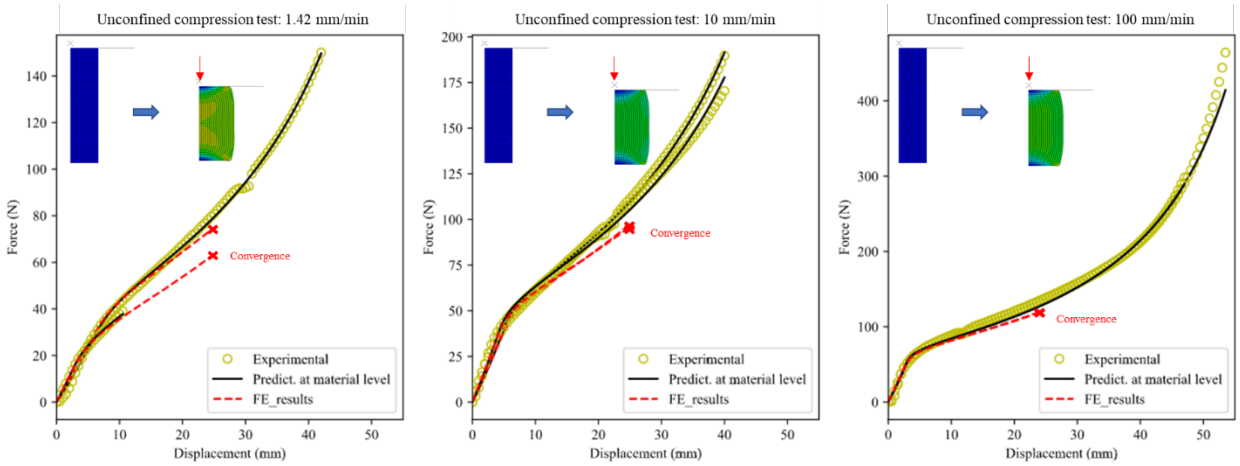

Figure 2. Comparison between experimental data and finite element results.

CONCLUSIONS

In this work, the mechanical properties of Crayola modeling clay are characterized via unconfined compression tests and inverse analysis. The proposed constitutive model with hardening can describe the finite elastoplasticity at substantial deformation. The inverse analysis using GA allows for determination of the material parameters, providing good agreement between experimental and predicted curves.

These results encourage future works involving the use of synthetic clay for completing experiments and prototyping technology designed to interact with soils (e.g., burrowing robot, model foundations, etc.). Crayola modeling clay can be used as an artificial soil for such experiments, and this paper provides a methodology for calibration of material parameters.

ACKNOWLEDGEMENT

This material is based upon work supported by the National Science Foundation under Grant No. 1830950.

REFERENCES

Del Dottore, E., Mondini, A., Sadeghi, A., Mattoli, V., and Mazzolai, B. (2016). "Circumnutations as a penetration strategy in a plant-root-inspired robot." *Proc. IEEE International Conference on Robotics and Automation*, IEEE, 2016-June, 4722–4728.

Iskander, M. G., Lai, J., Oswald, C. J., and Mannheimer, R. J. (1994). "Development of a transparent material to model the geotechnical properties of soils." *Geotechnical Testing Journal*, ASTM International, 17(4), 425–433.

Mishra, A. K., Tramacere, F., Guarino, R., Pugno, N. M., and Mazzolai, B. (2018). "A study on plant root apex morphology as a model for soft robots moving in soil." *PLoS ONE*, 13(6), 1–17.

Sadeghi, A., Tonazzini, A., Popova, L., and Mazzolai, B. (2013). "Robotic mechanism for soil penetration inspired by plant root." *Proc. IEEE International Conference on Robotics and Automation*, IEEE, 3457–3462.

Sadeghi, A., Tonazzini, A., Popova, L., and Mazzolai, B. (2014). "A novel growing device inspired by plant root soil penetration behaviors." *PLoS ONE*, 9(2), 1–10.

Simo, J. C. (1992). "Algorithms for static and dynamic multiplicative plasticity that preserve the classical return mapping schemes of the infinitesimal theory." *Computer Methods in Applied Mechanics and Engineering*, 99(1), 61–112.

Simo, J. C., and Meschke, G. (1993). "A new class of algorithms for classical plasticity extended to finite strains. Application to geomaterials." *Computational Mechanics*, 11(4), 253–278.

Tonazzini, A., Popova, L., Mattioli, F., and Mazzolai, B. (2012). "Analysis and characterization of a robotic probe inspired by the plant root apex." *Proc. IEEE RAS and EMBS International Conference on Biomedical Robotics and Biomechatronics*, IEEE, 1134–1139.